Physics of Fluids

Vortex dynamics and acoustic sources in the wake of finned cylinders during resonance excitation

Cite as: Phys. Fluids **32**, 075117 (2020); https://doi.org/10.1063/5.0016076
Submitted: 01 June 2020 . Accepted: 09 July 2020 . Published Online: 24 July 2020

Md Rashidul Islam, Mahmoud Shaaban, and Atef Mohany

View Online Export Citation CrossMark

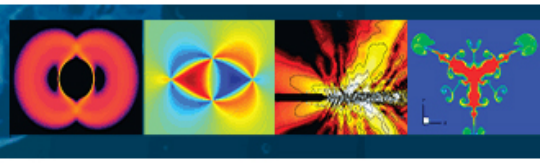
ARTICLES YOU MAY BE INTERESTED IN

Vortex shedding characteristics in the wake of circular finned cylinders
Physics of Fluids **32**, 045113 (2020); https://doi.org/10.1063/5.0005079

Influence of diametral acoustic mode on cavity flow dynamics: Zonal large eddy simulation and proper orthogonal decomposition
Physics of Fluids **32**, 075103 (2020); https://doi.org/10.1063/5.0012640

Spinning behavior of flow-acoustic resonant fields inside a cavity: Vortex-shedding modes and diametral acoustic modes
Physics of Fluids **32**, 085109 (2020); https://doi.org/10.1063/5.0019112

Physics of Fluids GALLERY OF COVERS



AIP Publishing

© 2020 Author(s).

Physics of Fluids ARTICLE scitation.org/journal/phf

Vortex dynamics and acoustic sources in the wake of finned cylinders during resonance excitation

Cite as: Phys. Fluids 32, 075117 (2020); doi: 10.1063/5.0016076
Submitted: 1 June 2020 • Accepted: 9 July 2020 •
Published Online: 24 July 2020

View Online Export Citation CrossMark

Md Rashidul Islam, Mahmoud Shaaban, and Atef Mohany[a)]

AFFILIATIONS

Aeroacoustics and Noise Control, Laboratory University of Ontario Institute of Technology, Oshawa, Ontario L1G 0C5, Canada

[a)]Author to whom correspondence should be addressed: atef.mohany@uoit.ca

ABSTRACT

The flow–sound interaction mechanism and its effect on the vortex dynamics in the wake of circular finned cylinders are experimentally investigated using phase-locked particle image velocimetry at Reynolds numbers between 7×10^4 and 9.5×10^4. In addition, a hybrid experimental–numerical technique using the theory of vortex sound is employed to quantify the acoustic sources and sinks in the vicinity of finned cylinders with different fin-to-root diameter ratios, D_f/D_r = 1.5, 2.0, and 2.5. The results show that changing the diameter ratio of the fins induces fundamental changes in the wake structure and the vortex shedding process downstream of the cylinder. Finned cylinders induce stronger vortex cores with a shorter formation length compared to their equivalent bare cylinders. Moreover, the flow topology over the spanwise direction shows that acoustic resonance results in uniform cylindrical vortex cores with less three-dimensional distortion, which demonstrates that the flow field becomes highly two-dimensional during resonance excitation. Quantification of the energy transfer between the flow and the sound fields reveals an enhancement in the acoustic energy production closer to the cylinder with a significant dependence on its fin-to-root diameter ratio.

Published under license by AIP Publishing. https://doi.org/10.1063/5.0016076

NOMENCLATURE

c	speed of sound in air
D	bare cylinder diameter
D_{eff}	effective diameter
D_f	fin diameter
D_r	root diameter
f	frequency of acoustic pressure fluctuations
f_a	acoustic cross-mode frequency
f_v	vortex shedding frequency
H	height of the duct
M	Mach number
P_{rms}	root mean square of the acoustic pressure signal
P^*	normalized acoustic pressure
s	fin pitch
t	fin thickness
U	velocity field
U_∞	inlet flow velocity
u_a	acoustic particle velocity
u_c	convection velocity
U_r	reduced flow velocity
v'	fluctuating transverse velocity
Γ	circulation of vortices
Π	acoustic power
ρ	density of air
ϕ	phase angle
ω	vorticity

I. INTRODUCTION

Flow-induced acoustic resonance is a design challenge in many engineering applications such as tube bundles in heat exchangers and boilers,[1,2] turbomachines,[3,4] piping systems,[5,6] side branches,[7–9] and reactor vessels.[10] It occurs when periodic flow instabilities couple with an acoustic mode. This often leads to the generation of acute noise problems and/or excessive vibrations that could result in catastrophic failures.[11] While this phenomenon is relatively well

Published under license by AIP Publishing

understood for bare cylinders in cross-flow, it remains unclear for the case of finned cylinders. Recent investigations[12] have shown that adding fins to a cylinder has a significant effect on the flow development around it. However, the effect of fins on the flow-acoustic coupling is not yet fully understood.

The pioneering work by Blevins and Bressler[1] identified the periodic vortex shedding in the wake of a bare cylinder as the source of resonance excitation. The vortex shedding in the wake induces velocity and pressure perturbations with spectral characteristics that are dependent on the flow velocity. Since the surrounding duct that encloses the cylinder contains acoustic modes with distinct frequencies, the frequency of the vortex shedding can coincide with the frequency of an acoustic mode of the duct at certain flow velocities. If the flow has enough energy to overcome the acoustic damping in the system, acute acoustic resonance can materialize. During resonance, the acoustic field oscillations grow stronger, and the acoustic particle velocity may reach a level up to 10% of the mean flow velocity, which strongly influences the vortex shedding process.[13] Moreover, the vorticity field can supply more energy to the acoustic field, which sustains resonance excitation over a range of flow velocities. This feedback cycle, which results in a positive energy transfer between the flow and the sound fields, is responsible for severe acoustic pressure fluctuations inside the duct, an enhancement in the fluid forces acting on the cylinder, and a stronger vorticity field.[13–15] Although the resonance excitation is relatively well understood for bare cylinders in cross-flow,[14,16–19] the addition of circular fins can severely alter the aforementioned mechanism of flow-acoustic coupling. This is because the resulting changes in the vortex dynamics with the addition of fins are bound to affect the characteristics of the acoustic source(s) in the flow field that are responsible for initiating and sustaining resonance excitation.

Several recent studies highlighted the significance of adding circular fins on the flow development downstream of the cylinders. McClure and Yarusevych[20] investigated the flow development and the structural loading on the circular finned cylinders with a different fin pitch. They reported significant changes in the mean drag, the vortex formation length, and the fluctuating lift force on the cylinder with a dependence on the fin pitch. Recently, Arafa and Mohany[21] experimentally and numerically investigated the effect of circular fins on the wake structure downstream of a single finned cylinder in cross-flow at a Reynolds number of 2.4×10^4. Their results showed that the spacing between the adjacent fins is critical to the flow development downstream of the cylinder. At lower fin spacing, they found that the flow is entrained between the fins, which results in the generation of an accelerated jet-like flow in the region between the fins, leading to a closer and stronger shear layer roll-up and hence a shorter vortex formation region. Moreover, the vortex shedding is found to be more correlated along the span of the finned cylinders as the fin spacing decreases. However, the vortex dynamics in the wake of the finned cylinders under resonant conditions and the aeroacoustic energy transfer were not investigated. Islam and Mohany[12] experimentally investigated the effect of the fin-to-root diameter ratio on the near wake flow development and the vortex shedding characteristics downstream of the circular finned cylinders using particle image velocimetry (PIV). They reported a significant reduction in the recirculation zone, in addition to an amplified primary vortex shedding process in the wake of the cylinders. Moreover, the amplification of the vortex shedding process led to enhanced velocity fluctuations due to a more coherent vorticity shedding in the wake of the finned cylinders for a higher diameter ratio. Islam and Mohany[12] also found that the fins have a significant effect on the strength and the convection velocity of the vortices in the wake. The observed changes were attributed to the higher flow entrainment between the fins. However, the investigation was carried out in the absence of acoustic resonance excitation. These fundamental changes in the vortex dynamics around the finned cylinders are bound to affect the aeroacoustics characteristics and the energy transfer mechanism during resonance excitation, which need to be investigated.

The available investigations in the literature on the flow excited acoustic resonance of the circular finned cylinders are scarce. Among the few available studies, some contradictory findings have been reported. Eid and Ziada[22] experimentally studied the effect of circular fins on vortex shedding and their role on the acoustic resonance excitation for single and two tandem cylinders at Reynolds numbers up to 10^5. For a single cylinder, they reported that the addition of fins results in a significant reduction in the acoustic pressure during resonance excitation. Based on the results obtained under non-resonant conditions, they attributed the weakened vortex shedding strength to the role of fins. Therefore, the vortex shedding resulted in a weaker excitation of the acoustic resonance compared with the bare cylinder. In contrast, Arafa and Mohany[23] reported a significant enhancement of the acoustic pressure fluctuations during resonance excitation for the circular finned cylinders compared to their equivalent bare cylinders. Moreover, they revealed that the amplitude of the excited acoustic resonance depends on the cylinder's aspect ratio, which was overlooked in the study of Eid and Ziada.[22] The combined effect of the shorter vortex formation length and higher spanwise correlation of the vortices is bound to instigate a stronger flow-acoustic coupling in the near wake of the finned cylinders. As mentioned earlier, the study by Islam and Mohany[12] found significant changes in the vortex shedding process downstream of the finned cylinders with different fin-to-root diameter ratios. However, their effect on the excitation mechanism of acoustic resonance has not been investigated. During resonance, the flow field becomes coupled with the acoustic field, which results in a direct energy transfer between them. To understand the energy transfer mechanism, it is imperative to identify the regions of acoustic energy generation in the wake. Using the aeroacoustic analogy, derived from Lighthill's theory of aerodynamic sound, Howe[24] showed that the acoustic energy generation requires the presence of a non-zero vorticity field. Later, Howe[25] provided a formula that enables the estimation of the energy transfer rate between the flow and acoustic fields. Howe's analogy has successfully been used to understand the energy transfer mechanism in the wake of bare cylinders[13,26,27] during self-excited and externally excited acoustic resonance. In addition to the resonant acoustic field, the application of Howe's analogy requires the knowledge of the flow field during resonance. However, the vortex dynamics in the wake of the circular finned cylinders in the presence of acoustic resonance have never been investigated to date. The excitation of acoustic resonance can be avoided by identifying the location(s) of the acoustic source(s) in the flow field and preventing the energy transfer between the flow and sound fields.

Additionally, there is a fundamental question related to the effect of acoustic resonance excitation on the three-dimensional flow

Published under license by AIP Publishing

topology around both bare and finned cylinders in cross-flow. The flow in the wake of a bare cylinder is known to be highly three-dimensional, even at low Reynolds numbers.[28] In the absence of acoustic excitation, instabilities result in vortex dislocations between spanwise cells of different frequencies when the primary vortices move out of phase with each other, and the wake pattern is dominated by the streamwise vortex pairs spaced by a distance of about one cylinder diameter.[29] In a fully turbulent flow, the organized structures in the nominally two-dimensional wake exhibit significant three-dimensionality even in the near field.[30] On the other hand, the presence of strong oscillations, such as those induced during self-excited acoustic resonance, has been observed to synchronize vortex shedding in other configuration.[31] Other flow features that induce regular fluctuations such as synthetic jets placed near the mean separation point of a bare cylinder have been used to inhibit the three-dimensionality of the near wake.[32] Although acoustic resonance is believed to induce strong synchronized fluctuations along the span of the cylinder, no experimental verification of the wake two-dimensionality is available in the literature. The confirmation of a two-dimensional vortex shedding process during self-excited acoustic resonance will facilitate an efficient way of modeling flow-acoustic coupling using the two-dimensional flow assumption. As a result, numerical investigations would require less computational capabilities to obtain results with reasonable accuracy.

The foregoing discussion reveals that the aeroacoustic coupling during self-excited resonance is not well understood in the case of circular finned cylinders in cross-flow. Moreover, the effect of fin-to-root diameter ratios on the vortex dynamics and the flow-acoustic coupling mechanism needs to be clarified. These shortcomings present a challenge that hinders the development of reliable control techniques that can be used to avoid the occurrence of acoustic resonance excitation in industrial applications. Therefore, this study focuses on the phase-locked vortex dynamics and its coupling with the acoustic field under resonant conditions. We consider the coupling between the flow field and the first acoustic standing wave mode of the duct as it is more susceptible to excitation at a lower flow velocity. The characteristics of the self-excited resonance are identified from the acoustic pressure measurement over a range of flow velocities. Phase-locked PIV measurements are performed to resolve the unsteady vortex dynamics in the wake of the cylinder with respect to the acoustic pressure cycle. The resulting flow fields from the experiments are combined with the resonant sound field obtained from numerical simulations to determine the acoustic sources and sinks using Howe's analogy. Moreover, we performed phase-locked PIV measurements at several places along the span of the cylinder to elucidate the spanwise development of the vortices in the wake during acoustic resonance excitation.

II. METHODOLOGY

Experimental measurements of flow and acoustic variables are performed in an open-loop suction-type wind tunnel. The airflow in the tunnel is driven by a centrifugal air blower at the exit of the tunnel. Airflow enters through a bellmouth section to maintain a uniform flow before entering the test section of height 254 mm and width 127 mm. The test section is followed by a diffuser with a gradual increase in cross-sectional area to minimize the pressure drop in the tunnel. The diffuser is connected to the blower using a flexible connection, and the setup is rigidly mounted on supports designed to minimize external vibration. Figure 1(a) shows a schematic of the experimental setup. The cylinder is rigidly mounted with its axis aligned along the horizontal symmetry plane of the test section, which corresponds to the acoustic particle velocity antinodal plane of the first acoustic cross-mode inside the duct. Three cylinders with equispaced annular fins in addition to one bare cylinder are investigated in the current study. The length of all finned cylinders is 127 mm, spanning along the width of the test section. The spacing between the fins is 1.5 mm, which is the same for all the cylinders. The first effective fin at both ends of the cylinder is located 3 mm from the side walls. Measurements of the surface pressure on the bare cylinder were carried out over a range of Reynolds number between Re = 1.3×10^4 and 6.4×10^4 to verify the uniformity of flow conditions along the span of the cylinder. The base pressure coefficient was measured using pressure taps along the span of the cylinder at 180° from the upstream stagnation point. The base pressure coefficient was found to be uniform within 4% of its mean value over 94% of the cylinder's span. The profiles of the pressure coefficient over the circumference of the cylinder at its mid-span and near the side walls agree well with the measurements of Norberg.[33] The flow velocity inside the tunnel is controlled using a variable frequency drive and calibrated using a Pitot tube installed upstream of the cylinder location. The Pitot tube is

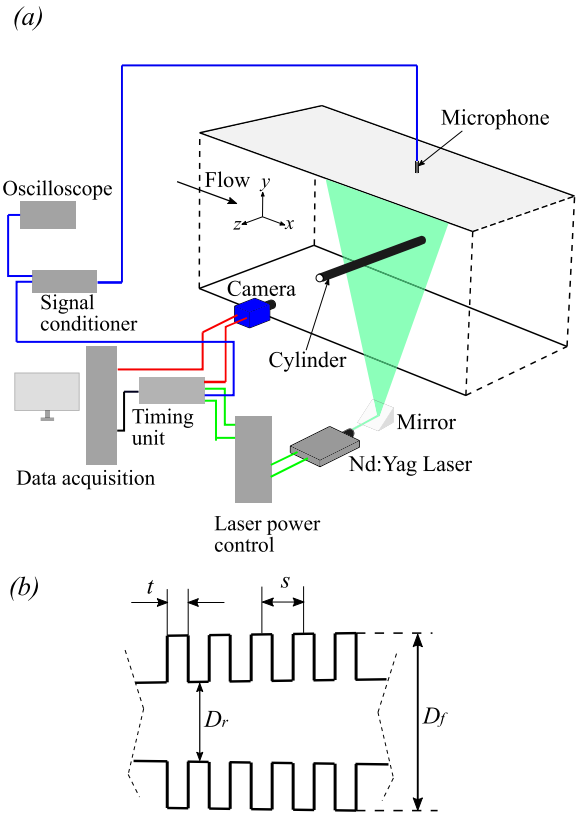


FIG. 1. (a) Schematic of the experimental setup (not to scale) and (b) cross-sectional view of the finned cylinder geometry with nomenclature.

Published under license by AIP Publishing

removed after calibration to eliminate any disturbance during flow and acoustic measurements. Hotwire measurements with no cylinder attached indicated a maximum free-stream turbulent intensity of ≈0.7%.

Figure 1(b) shows a schematic of the finned cylinder cross-section and the nomenclature used to define its characteristic geometrical parameters. Three finned cylinders with the same fin pitch (s), the same fin thickness (t), and different diameter ratios (D_f/D_r) are investigated. The non-dimensional geometric parameters considered for the finned cylinders in the current study are within the range commonly found in industrial applications. The effective diameter D_{eff}, defined in Eq. (1), is kept constant at D_{eff} = 19.05 mm for all the finned cylinder cases to form a basis for flow field comparison with the same flow blockage. The form of the effective diameter in Eq. (1) was proposed by Mair and Jones[34] taking into account the frontal area flow blockage provided by the finned cylinder model. Measurements were carried out for a bare cylinder with a diameter equal to the effective diameter of the finned cylinders to provide a base case for the flow field and acoustic resonance excitation. The dimensions of the geometrical parameters used for the finned cylinders are summarized in Table I,

$$D_{\text{eff}} = \frac{1}{s}\left[(s-t)D_r + tD_f\right]. \tag{1}$$

A. Aeroacoustic measurement

To measure the aeroacoustic response, the acoustic pressure signal is recorded at different flow velocities between 20 m/s to 100 m/s. The corresponding Reynolds number ranges between Re = 2.55 × 10^4 and Re = 1.27 × 10^5 based on the effective diameter and the free-stream flow velocity used in the measurements. Vortex shedding causes periodic pressure fluctuations normal to both the axis of the cylinder and the flow direction, resembling a dipole sound source. Therefore, only transverse acoustic modes with acoustic pressure antinodes on the walls parallel to the cylinder axis can be excited. The excitation of the acoustic mode with the lowest frequency is of interest in the current study, as it will occur at the lowest excitation flow velocity. Figure 2 shows the normalized acoustic pressure distribution of the first acoustic cross-mode in the duct obtained from the finite element analysis, as will be discussed later. The cylinder is located at the pressure node of the resonant standing wave. Acoustic pressure measurements are carried out using a pre-polarized pressure microphone (1/4 in.) flush-mounted at the top wall of the test section at the location of the maximum acoustic pressure. The microphone is attached 1 in. downstream from the center of the cylinder, experimentally determined as the location of maximum acoustic pressure recorded during the excitation

TABLE I. Geometrical parameters of the investigated cylinders; all cylinders have D_{eff} = 19.05 mm.

	D_r (mm)	D_f/D_r	s/D_{eff}	t/D_{eff}
Finned cylinder I	15.24	1.50	0.158	0.079
Finned cylinder II	12.70	2.00	0.158	0.079
Finned cylinder III	10.89	2.50	0.158	0.079

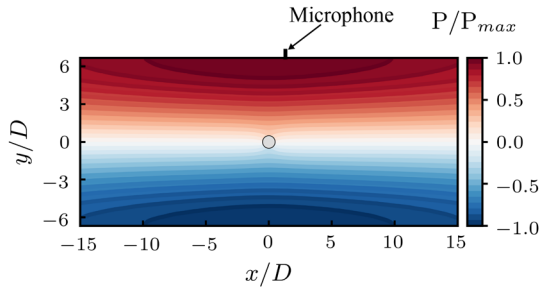


FIG. 2. Normalized pressure distribution of the first acoustic standing wave mode.

of acoustic resonance.[35] The pressure signal is recorded for a duration of 120 s at a sampling frequency of 20 kHz. The frequency spectrum is calculated using Welch's modified periodogram method with a 50% overlap and a frequency resolution of 1 Hz. The microphone signal is filtered using a fourth-order Butterworth filter with a frequency bandwidth of ±50 Hz around the dominant frequency peak. The value of the acoustic pressure P_{rms} is calculated from the root mean square (rms) of the filtered acoustic pressure signal. An approximate value of the natural frequency of the first acoustic cross-mode can be obtained from the following equation:

$$f_a = \frac{c}{2H}, \tag{2}$$

where c is the speed of sound and H is the height of the duct. The value of f_a calculated using Eq. (2) is 675 Hz, which falls within 2% of the measured experimental frequency during resonance excitation. In order to compare the aeroacoustic response of different cylinders, the acoustic pressure is presented in a normalized form, P^*, scaling the aerodynamic pressure oscillations with the input kinetic energy and the Mach number according to the theory of aeroacoustic sound,[36,37]

$$P^* = \frac{2P_{\text{rms}}}{\rho U_\infty^2 M}, \tag{3}$$

where M is the Mach number of the mean flow at the inlet. The flow velocity is normalized in the form of reduced velocity (U_r), defined as

$$U_r = \frac{U_\infty}{f_a D_{\text{eff}}}. \tag{4}$$

B. Phase-locked particle image velocimetry

To investigate the effect of the fin diameter ratio on the unsteady flow field during resonance, phase-locked PIV measurements are carried out in vertical planes that span the x–y direction, as shown in Fig. 1(a). The peak acoustic pressure level during resonance excitation occurs at Reynolds numbers between 7 × 10^4 and 9.5 × 10^4 for the tested cases. A pulsed Nd:Yag laser with a wavelength of 532 nm is used to illuminate the flow field. A CCD camera is used to capture images of the illuminated measurement plane at a resolution of 2752 × 2200 pixel. The airflow is seeded with

Published under license by AIP Publishing

particles of bis(2-ethylhexyl) sebacate (DEHS) generated using an aerosol generator at a mean particle diameter of ~1 μm. The PIV measurements for different cases are carried out at a flow velocity that corresponds to the maximum P_{rms} recorded during resonance excitation.

For the finned cylinders, the measurement planes are located at the center of the spacing between two consecutive fins close to the midspan of the cylinder. In addition, to characterize the spanwise flow development in the wake of the cylinders during resonance, PIV measurements are performed at multiple x–y planes located along the span of the cylinders. The spanwise measurements are performed for the bare cylinder and one representative case of the finned cylinder with $D_f/D_r = 2.0$ at the same phase of the acoustic pressure cycle. The measurements are performed over a region of $3D_{\text{eff}}$ along the span. A traverse mechanism is used to precisely control the spanwise locations of the measurement planes that are separated by a distance of $\Delta z = 9.5$ mm

The signal from the flush-mounted microphone at the acoustic pressure anti-node of the test section is used to trigger the laser pulse. The laser timing system shoots the laser and captures image pairs at a preset delay after the pressure signal trigger. This enables the acquisition of image pairs that correspond to the same phase instants of the acoustic pressure cycle. As the frequency of the acoustic mode is higher than the maximum laser shooting frequency, several vortex shedding cycles are skipped between consecutive image pairs. However, the periodic vortex shedding influenced by strong steady pressure oscillations under the lock-in condition ensured that image pairs are captured at the desired phase angle with a minimum uncertainty. To modify the phase of the flow field relative to the acoustic cycle, the delay between the trigger signal and the image acquisition is adjusted using a timing circuit. Measurements are taken at eight uniformly spaced phases of the acoustic pressure cycle. For each phase, 100 instantaneous pair of images are acquired. The time between pulses is adjusted to capture the maximum particle displacement within one-quarter of the interrogation window used for vector calculation. To minimize the effect of any jitter due to measurements in different planes away from the microphone location, 500 instantaneous pair of images are acquired at each plane for the measurements performed along spanwise locations. Images are preprocessed to reduce any spurious reflections in the acquired images followed by intensity normalization. Moreover, the areas affected by the shadow of the cylinder and near the boundaries of the field of view are excluded from the analysis. The vector field calculations are performed using the multipass cross-correlation algorithm with one pass at an initial window size of 48 × 48 pixels with 50% overlap and four final passes at an interrogation window size of 24 × 24 pixels with 50% overlap. The final vector fields have a vector pitch of $0.06D \times 0.06D$. The measurement of flow velocity $\vec{v}$ is accurate within ±4%, and the acoustic pressure P_{rms} is measured with an uncertainty of ±0.9%.

C. Quantification of local acoustic energy transfer

The aeroacoustic energy transfer between the flow and the acoustic field of the standing wave is quantified using Howe's integral formulation of the aerodynamic sound[25] using a hybrid numerical–experimental model. The general formulation of the theory of aerodynamic sound [Eq. (5)] estimates the sound radiated from fluid flow,

$$\frac{\partial^2 \rho}{\partial t^2} - c_0^2 \nabla^2 \rho = \frac{\partial^2}{\partial x_i \partial x_j}\left(\rho v_i v_j + p_{ij} - c_0^2 \rho \delta_{ij}\right), \tag{5}$$

where the density ρ fluctuates according to the second-order spatial gradient of the turbulent stress tensor in the right-hand term. The complexity of obtaining closure for the solutions of Eq. (5) is expected as this formulation is an integral form of the Navier–Stokes equation, where the source term accounts for the generation of sound in addition to self-modulation due to acoustic non-linearity, convection by the flow, refraction due to sound speed variations, and attenuation caused by thermal and viscous effects. For relatively simple, incompressible flows at low Mach numbers and neglecting nonlinear aerodynamic and flow phenomena, Howe[38] showed that the sound generation by the fluctuating fluid forces caused by a vorticity field can be modeled as a dipole source. For an incompressible flow field with vorticity ω, acoustic particle velocity u_a, and flow velocity U, the acoustic pressure p emitted by a local dipole source can be calculated according to the following equation:

$$\frac{\partial^2 p}{\partial^2 t} - \nabla^2 p = c_0 \rho_0 \nabla.(\vec{\omega} \times \vec{u_a}). \tag{6}$$

The instantaneous acoustic power Π is obtained from the instantaneous flow velocity $\vec{U}$, instantaneous flow vorticity $\vec{\omega}$, and the instantaneous acoustic particle velocity $\vec{u_a}$ according to the following equation:

$$\Pi = -\rho \int \vec{\omega} \cdot (\vec{U} \times \vec{u_a}) d\forall. \tag{7}$$

This analytical derivation forms an acoustic analogy of sound generation by fluid flow, where sound fields are directly related to integrals of surface and volume source terms. The algorithm used in this work to compute the spatial distribution of the acoustic energy transfer rate and deduce the location and strength of acoustic sources and sinks is shown in Fig. 3. To identify the local acoustic source strength, the interaction of the flow velocity, the flow vorticity, and the acoustic particle velocity is needed. The acoustic pressure (P_{rms}) is obtained experimentally from the aeroacoustic response measurement, as described before. The two-dimensional fields of velocity $\vec{U}$ are obtained at eight phases of the acoustic pressure cycle using the phase-locked PIV measurements. Vorticity ($\vec{\omega}$) around the spanwise axis is measured from the velocity vectors using the eight-point circulation method.[39] The two-dimensional distribution of acoustic particle velocity over the same plane is obtained using finite element analysis, as will be discussed next.

A three-dimensional eigenvalue modal analysis is performed to obtain the planar acoustic particle velocity vector distribution at a plane corresponding to the PIV measurement plane. A finite element solution is carried out to obtain the acoustic pressure and the vectors of acoustic particle velocity for the first acoustic transverse mode by solving the Helmholtz equation given as

$$\nabla^2 \varphi + k^2 \varphi = 0, \tag{8}$$

where $k = 2\pi f_a/c$ is the wavenumber. During self-excitation of acoustic resonance, the time variation in the acoustic pressure $p(t)$ inside

Published under license by AIP Publishing

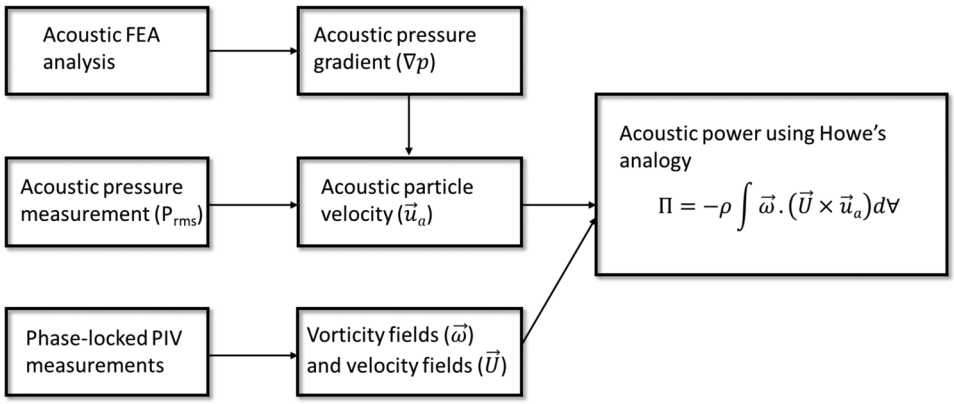


FIG. 3. Algorithm used to quantify local acoustic power production.

the duct can be modeled as a simple harmonic motion according to the following equation:

$$p(t) = \varphi e^{i(2\pi f_a)t}. \tag{9}$$

The variable φ satisfies the Helmholtz equation given in Eq. (8). Equations (8) and (9) are solved with the appropriate boundary conditions over a three-dimensional domain representing the experimental test section. The inlet and the outlet are placed $60D_{\text{eff}}$ upstream and downstream from the center of the cylinder, respectively, to implement the zero acoustic pressure at the boundaries. The discretization of the numerical grid is performed using a linear acoustic element. The planar acoustic pressure distribution is calculated from the three-dimensional results at the plane of measurements in a normalized form. Therefore, the acoustic pressure is scaled using the measured P_{rms} value for each case. The Euler equation given in Eq. (10) relates the acoustic particle velocity distribution to the distribution of the acoustic pressure in the domain,

$$\rho \frac{\partial \vec{U}_a}{\partial t} = \nabla p. \tag{10}$$

The acoustic particle velocity field $\vec{U}_a$ is obtained using the integral of the Euler equation,

$$\vec{U}_a(x,y,z) = \frac{P_{\text{rms}} \cdot \nabla p(x,y,z)}{2\pi \cdot \rho \cdot f_a}, \tag{11}$$

where P_{rms} is the measured acoustic pressure and $p(x, y, z)$ is the normalized pressure distribution obtained from the numerical calculations at a plane with the same spanwise location (z) as the PIV measurement plane. Under resonant conditions, the acoustic particle velocity of the resonant mode lags the acoustic pressure by a phase angle of 90°. Thus, the acoustic particle velocity field is adjusted to obtain the instantaneous distribution corresponding to the phase of the acoustic pressure cycle as

$$\vec{u}_a(x,y,z,t) = \vec{U}_a \sin\left(2\pi f_a t + 90^\circ\right). \tag{12}$$

The obtained flow and acoustic quantities are then used in Eq. (7) to calculate the instantaneous energy production $\Pi(x, y, t)$ at all phase instants.

III. AEROACOUSTIC CHARACTERISTICS

In this section, the aeroacoustic response of the finned cylinders in cross-flow is presented to identify the effect of the diameter ratio (D_f/D_r) on the acoustic resonance excitation. For this purpose, the characteristics associated with the amplitude and the dominant frequency of the acoustic pressure fluctuations measured for a range of incoming flow velocities are discussed. In Figs. 4(a) and 4(c), the spectrogram of the measured acoustic pressure fluctuations in the case of the bare cylinder before and during the excitation of acoustic resonance is shown. At a flow velocity of $U_\infty = 41.6$ m/s, lower than that necessary for the onset of acoustic resonance, the spectrogram in Fig. 4(a) shows two distinct frequency bands with a high spectral energy. Among them, the dominant frequency in pressure fluctuations is $f = 435$ Hz, which corresponds to the non-dimensional Strouhal number of $St = 0.198$. This value of the Strouhal number is typical for the periodic fluctuations of vortex shedding in the wake of a bare cylinder at this range of Reynolds numbers. A close inspection of Fig. 4(a) shows that the spectral energy is distributed around a band of frequencies near the dominant peak, $f_v = 435$ Hz, implying a temporal variation in the periodicity of vortex shedding. Moreover, the existence of spectral energy around a frequency band near the peak of $f_a = 670$ Hz is also evident from Fig. 4(a), which corresponds to the natural frequency of the first acoustic cross-mode of the duct housing the cylinder. In comparison, when acoustic resonance is initiated at $U_\infty = 67$ m/s, the spectrogram exhibits one dominant peak near $f_a = 670$ Hz in Fig. 4(c), which indicates the occurrence of the frequency coincidence that is typical during acoustic resonance excitation. Moreover, the spectral energy during resonance in Fig. 4(c) is mostly concentrated around the dominant peak, $f_a = 670$ Hz, indicating the presence of an amplified periodic phenomenon. This enhanced periodicity of the pressure fluctuations results from the coupling between the aerodynamic and acoustic fields during resonance. For the finned cylinder with $D_f/D_r = 2.0$, the spectrogram of the measured acoustic pressure signal is shown in Figs. 4(b) and 4(d) to get insight into the spectral characteristics before and during resonance excitation. The spectrogram before resonance exhibits two peaks similar to that of the bare cylinder. However, the spectral energy shows variation over a narrower region around the peak of the vortex shedding frequency, $f_v = 446$ Hz, implying an increased periodicity of the fluctuations compared to that of the bare cylinder.

Published under license by AIP Publishing

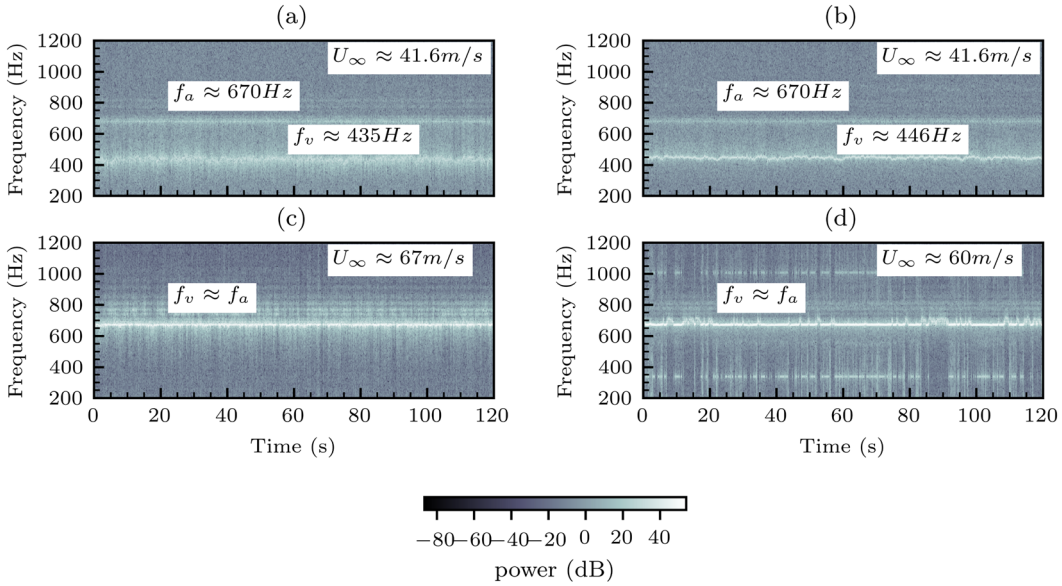


FIG. 4. Spectrogram of the acoustic pressure fluctuations recorded before the onset of resonance and during resonance. [(a) and (c)] Bare cylinder and [(b) and (d)] finned cylinder, D_f/D_r = 2.0.

Moreover, the spectral energy of the coincided frequency during resonance in Fig. 4(d) exhibits enhanced periodicity of fluctuations, as a result of the coupling with the resonant acoustic field. The spectrogram reveals that a fundamental change occurs in the spectral characteristics of the acoustic pressure fluctuations under acoustic resonance excitation.

To understand the salient characteristics associated with the excitation of acoustic resonance, the spectra of the acoustic pressure fluctuations for a range of flow velocities are inspected in Fig. 5(a). The waterfall spectra of the acoustic pressure fluctuations in the case of the bare cylinder are shown. At lower flow velocities, the spectra of the pressure fluctuations have two discernible peaks, although not readily apparent in Fig. 5(a) due to the relatively low amplitude. The two peaks correspond to the frequency of the vortex shedding and the natural frequency of the acoustic mode, as observed earlier. When the vortex shedding frequency becomes close to the natural frequency of the acoustic mode, a resonant acoustic standing wave forms inside the duct. As a result, the vortex shedding frequency (f_v) and the acoustic mode frequency (f_a) get synchronized, which is known as the frequency "*lock-in*."[36] Following the excitation of the acoustic resonance, a feedback mechanism is initiated and results in energy exchange between the unsteady flow field and the resonant sound field. This feedback mechanism causes a sudden increase in the amplitude of fluctuating pressure inside the duct in the order of the dynamic head of the flow, as evident from Fig. 5(a). This state of acoustic resonance is self-sustained over a range of flow velocities between ≈63 m/s to ≈75 m/s. During this period, the vortex shedding frequency becomes locked-in to the first acoustic cross-mode frequency f_a = 670 Hz. The acoustic pressure falls to its previous level after the *lock-in* period. The dominant frequency and root mean square (rms) amplitude of the acoustic pressure fluctuations from each spectrum are extracted and plotted in Fig. 5(b), which delineates their progression with the increasing flow velocity. The P_{rms} value is obtained from the root mean square of the acoustic pressure signal bandpass filtered around the dominant frequency, as mentioned earlier. The line fit through the dominant frequency in the pressure spectra results in a Strouhal number value of $St \approx 0.20$, which corresponds to the periodic vortex shedding in the wake of a bare cylinder at this Reynolds number range.

Figure 6 presents the spectral map of the acoustic pressure signal for the finned cylinders along with the bare cylinder. The spectral maps show the variation in the Power Spectral Density (PSD) of the measured acoustic pressure signal over the range of flow velocities. The excitation of acoustic resonance near the frequency of the first acoustic mode occurs for all the finned cylinder cases, as evident from Figs. 6(b) and 6(c). The cases of finned cylinders show similar characteristics to each other but exhibit a significant difference with the case of the bare cylinder. In particular, the high-intensity fluctuations persist over a reduced range of flow velocities for the finned cylinders, compared to that of the bare cylinder, i.e., a narrower lock-in region. To delineate the differences in the aeroacoustic response, the progression of the normalized dominant frequency (f_v/f_a) and the normalized acoustic pressure (P^*) with the reduced flow velocity U_r is shown in Fig. 7. The normalized frequency for the finned cylinders in Fig. 7(a) exhibits similar trends to the bare cylinder. Likewise, the dominant frequency of acoustic pressure fluctuations for the finned cylinders increases linearly with the increase in the reduced flow velocity until the resonance is excited, and the "lock-in" condition is initiated. The linear fit through the dominant frequencies for the finned cylinders resulted in a Strouhal number value of $St \approx 0.20$, which is associated with the periodic vortex shedding in the wake.[12] Moreover, the frequency response in Fig. 7(a) also exhibits the occurrence of an earlier exit of the frequency from the "lock-in"

Published under license by AIP Publishing

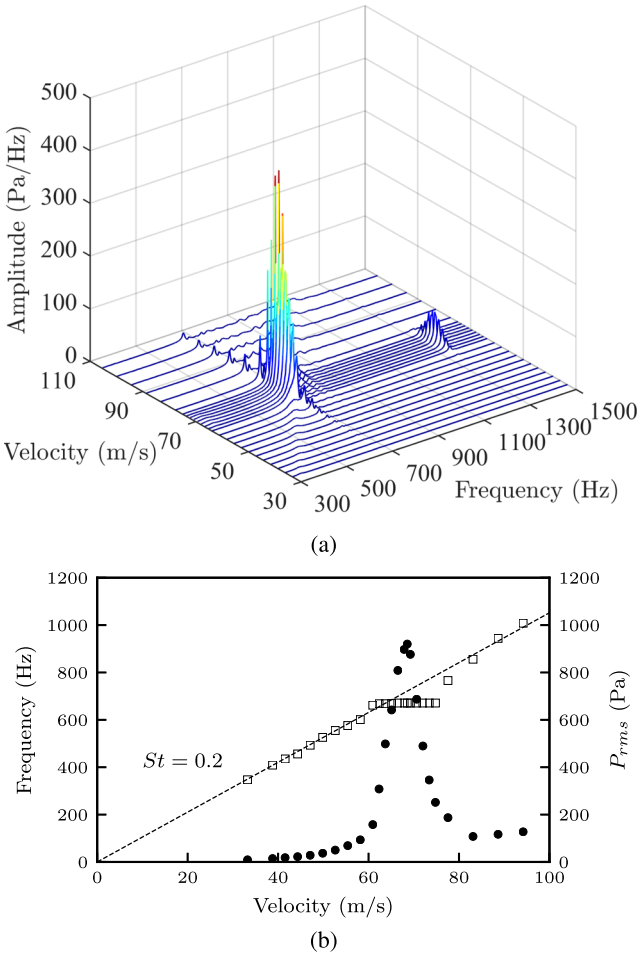


FIG. 5. The aeroacoustic response of a single bare cylinder: (a) waterfall plot of the acoustic pressure spectrum at different flow velocities and (b) the effect of the flow velocity on the dominant frequency and the root mean square acoustic pressure.

state in the case of the finned cylinders, resulting in a much shorter "lock-in" period, compared to that of the bare cylinder. Figure 7(b) shows that the acoustic resonance for all the finned cylinder cases was self-excited at a lower reduced flow velocity compared to that of the bare cylinder. Although the flow-acoustic coupling is sustained over a shorter range of flow velocities for the finned cylinder cases, Fig. 7(b) shows that the peak amplitude of P^* reaches a higher value than for the bare cylinder. Among the finned cylinders, the reduced velocity at the onset of the acoustic resonance and the peak normalized pressure during resonance shows a distinct variation. The onset of the excitation of the acoustic resonance gradually decreases from $U_r = 4.73$ to $U_r = 4.62$ as the diameter ratio increases from $D_f/D_r = 1.5$ to 2.5. The increase in the diameter ratio of the finned cylinder from $D_f/D_r = 1.5$ to 2.0 results in an increase in the normalized acoustic pressure generated during the resonance to a value of $P^* = 2.51$. However, a further increase in the diameter ratio from $D_f/D_r = 2$ to 2.5 causes a decrease in the normalized pressure to $P^* = 2.05$ at its peak value during resonance excitation.

In summary, the observations reveal that the characteristics of the acoustic resonance excitation for the finned cylinders significantly differ from those of the bare cylinder with the same effective diameter. The difference implies a fundamental change in the characteristics of the excitation source, which, in the present case, is the periodic vortex shedding. In the absence of acoustic resonance, previous studies[12,21] have found that the addition of fins around the bare cylinder has a profound impact on the wake vortex shedding characteristics. Arafa and Mohany[21] reported that the spanwise coherence of the vortex shedding along the span of the finned cylinder of a comparable fin pitch increases significantly than that of the bare cylinder under non-resonant conditions. Moreover, the strength of the vortices increases significantly due to the addition of fins.[12] Under resonance excitation, those effects, originating from the addition of fins, are expected to be accentuated. The enhanced spanwise coherence and stronger vortices are likely to cause the generation of a higher sound pressure level during resonance, as observed in the aeroacoustic response. On the other hand, the increase in fin diameter in the present case makes the onset flow velocity of the resonance excitation much lower than the bare cylinder, despite the usage of the same effective diameter (D_{eff}). The excitation at a lower flow velocity implies that the flow development in between the fins significantly affects the wake vortex shedding and therefore the resonance excitation. Indeed, the entrainment of flow between the fins results in an accelerated jet-like flow due to the presence of the lateral boundary layer on the surface of the fins.[21] Moreover, Islam and Mohany[12] reported an amplification of the coherent velocity fluctuations due to the vortex shedding process in the wake of the finned cylinders with increasing diameter ratios. The combined effect of the accelerated flow and enhanced coherent velocity fluctuation would result in higher perturbation in the near wake of the finned cylinder, where stronger flow-acoustic coupling takes place. The accelerated flow means that the local flow velocity at certain locations around the cylinder can be significantly higher than the upstream velocity, as opposed to the case of a bare cylinder. The result is an increased susceptibility to acoustic resonance, which causes the excitation at a lower upstream flow velocity, as observed in the aeroacoustic response. Despite the excitation at lower flow velocities, the acoustic resonance for the finned cylinders is sustained over a much shorter period of flow velocities than that of the bare cylinder due to the enhanced flow separation from the surface and edges of the fins as the diameter ratios increase, which would result in the generation of stronger secondary vortices near the surface of the fins. The interaction between the secondary vortices and the resonant sound field interrupts the coupling of the primary vortices at a higher pace as the flow velocity deviates from the condition of frequency coincidence. Another reason for the observed aeroacoustic response of the finned cylinders is the absorption of sound at the edges of the fins due to the enhanced flow separation from the fin surfaces. Howe[25] discussed that the presence of sharp edges at which mean flow separation occurs can cause a significant dissipation of the sound energy, which is expended at the production of vortices at the solid boundaries. To sustain acoustic resonance, the net generation of the aeroacoustic energy needs to be positive over the acoustic cycle. The enhanced sound energy absorption at the fin edges would cause a premature interruption of the sustenance of resonance. As evident from this discussion, the characteristics of flow-acoustic coupling around the finned cylinders appear to be

Published under license by AIP Publishing

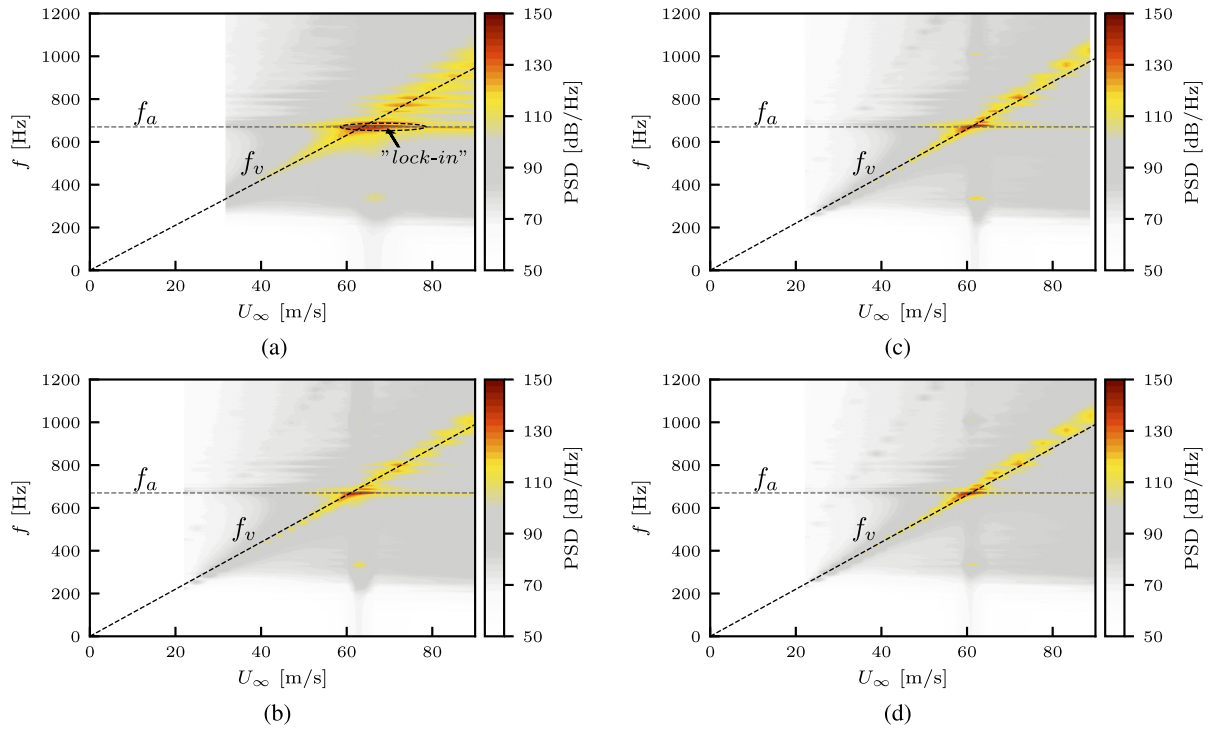


FIG. 6. Spectral characteristics of the acoustic pressure for the investigated cylinders over a range of flow velocities. (a) Bare cylinder, (b) D_f/D_r = 1.5, (c) D_f/D_r = 2.0, and (d) D_f/D_r = 2.5.

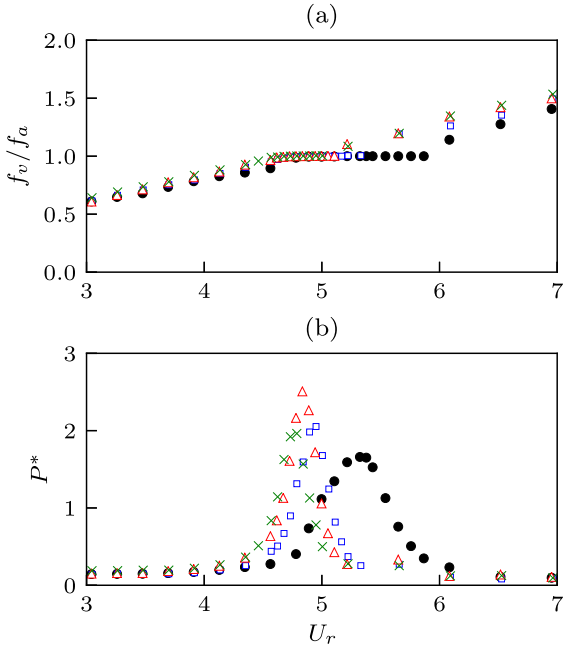


FIG. 7. The effect of the reduced flow velocity U_r on (a) the frequency ratio (f/f_a) and (b) the normalized acoustic pressure (P^*): (black circles) bare cylinder, (blue squares) D_f/D_r = 2.5, (red triangles) D_f/D_r = 2.0, and (green crosses) D_f/D_r = 1.5.

highly sensitive to the fin-to-root diameter ratio, leading to a significant effect on their aeroacoustic response. In addition, changes to the dynamics of the vortex shedding process plays a significant role, as will be discussed next.

IV. VORTEX DYNAMICS IN THE WAKE DURING ACOUSTIC RESONANCE

A. Vortex dynamics in the streamwise–transverse plane at the midspan

In this section, the phase-resolved flow field characteristics are discussed to provide insight into the vorticity dynamics and its influence on the excitation of the acoustic resonance. The cylinder is located at the acoustic pressure node of the first transverse acoustic standing wave mode, which is also the location of the antinode of the acoustic particle velocity. Therefore, the frequency coincidence results in amplified cross-flow oscillations due to the formation of the standing wave. According to the theory of vortex sound,[25] the vortices in the wake of the cylinder act as a source that transfers energy from the flow field to the acoustic field. Therefore, the vorticity field is the main driving force for the sustenance of the resonance, and understanding the vortex shedding characteristics is crucial to get insight into the flow-acoustic coupling.

In Fig. 8, the phase-resolved vorticity fields downstream of the bare cylinder at the midspan plane (z = 0) are plotted. The vorticity field shows a typical vortex shedding process downstream of the

Published under license by AIP Publishing

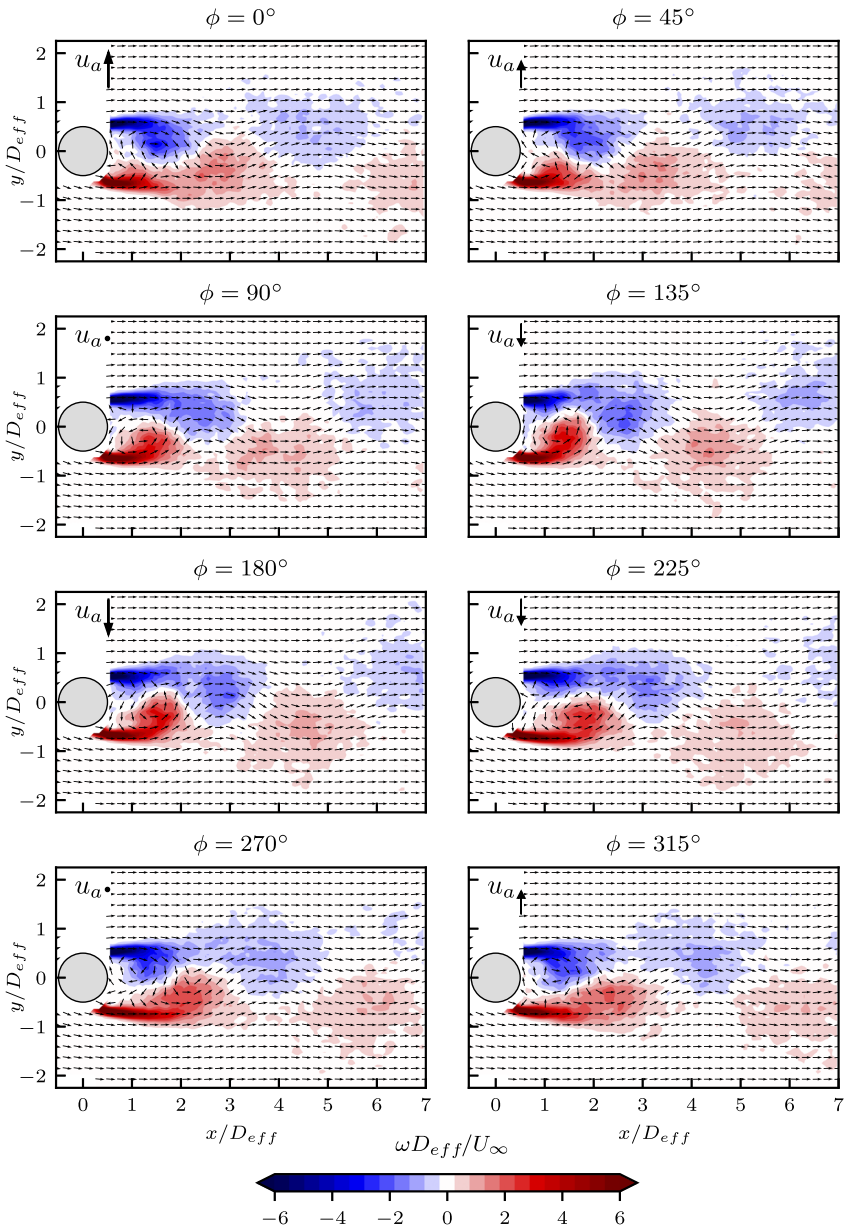


FIG. 8. Phase-resolved velocity vectors and vorticity field over a complete acoustic pressure cycle in the wake of a bare cylinder during excitation of acoustic resonance.

bare cylinder. At $\phi = 0°$, the incipient vortex core at the top shear layer forms due to the roll-up of vortices in the shear layer. This process continues over the phases $\phi = 45°$ and $\phi = 90°$. Meanwhile, the bottom shear layer moves toward the opposite direction due to the entrainment by the top shear layer. Careful consideration of the direction of the acoustic particle velocity u_a, which is shown at an arbitrary scale, shows that as the core of the vortex forms on one side of the cylinder, the acoustic particle velocity tends to flow to the other side, enhancing the separation process. As the acoustic field and the flow field are in the lock-in state, the phase between the fluctuating lift force and the acoustic velocity plays a crucial role in the energy transfer between the two fields, sustaining the resonant field. The vortex core is found to shed at the phase $\phi = 135°$, and after that, it convects downstream by the mean flow. The same process repeats for the other half of the cycle. As the vortices travel downstream, their vorticity content diffuses gradually, confirming that the effect of the flow-acoustic coupling is pronounced near the cylinder surface.

Figure 9 shows the phase-resolved vorticity field in the wake of the finned cylinder with $D_f/D_r = 2.0$. As this case locks-in to the same acoustic mode frequency as that in Fig. 8, the eight phases shown for both cases have the same temporal step. However, the addition of fins around the bare cylinder causes significant changes in the wake vortex structure. Vortices shed downstream of the finned cylinder

Published under license by AIP Publishing

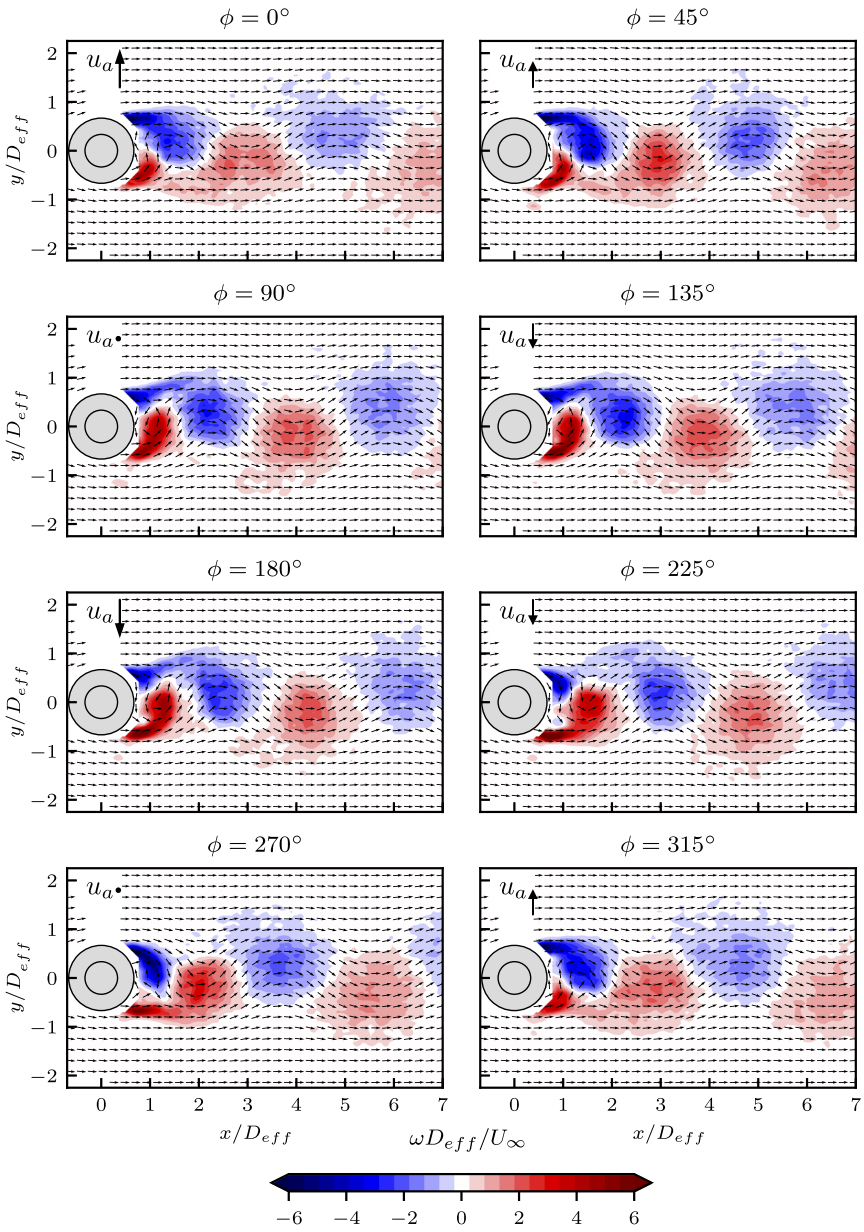


FIG. 9. Phase-resolved velocity vectors and vorticity field corresponding over a complete acoustic pressure cycle in the wake of the finned cylinder with D_f/D_r = 2.0 during excitation of acoustic resonance.

exhibits enhanced vorticity content and are more uniform with less distortion of their cylindrical structure. The vortex formation region moves upstream so that the number of vortex cores within the same downstream distance is higher for the finned cylinder. As the production of acoustic energy is more efficient closer to the cylinder surface, the shorter formation of stronger vortices is likely to result in an enhancement of the flow-acoustic coupling in the near wake.

The behavior of the vortices in the wake of each cylinder plays a significant role in the excitation of acoustic resonance and the aeroacoustic energy transfer. To compare the strength and the decay rate of the vortices for the investigated cylinders, the circulation of the bounded vortex region is quantified. To identify individual vortices, each connected circulating region is distinguished from the rest of the flow fields using the Q-criterion.[40] Vortices are identified as the region where the normalized second positive invariant, Q, of the velocity gradient tensor $\nabla\vec{U}$ is higher than 0.005. This threshold was selected as an optimal value below which the change in circulation is negligible. To improve the consistency of the identification criterion, the Gaussian Mixture Model (GMM) is used to fit a continuous bounded ellipse based on the mean and covariance of the sub-population, which, in the present case, is the vorticity region identified using $Q > 0.005$. The approach provides a robust criterion for selecting the region consistently, for the computation of the circulation.[41] The identified vorticity regions such as those in Fig. 10

Published under license by AIP Publishing

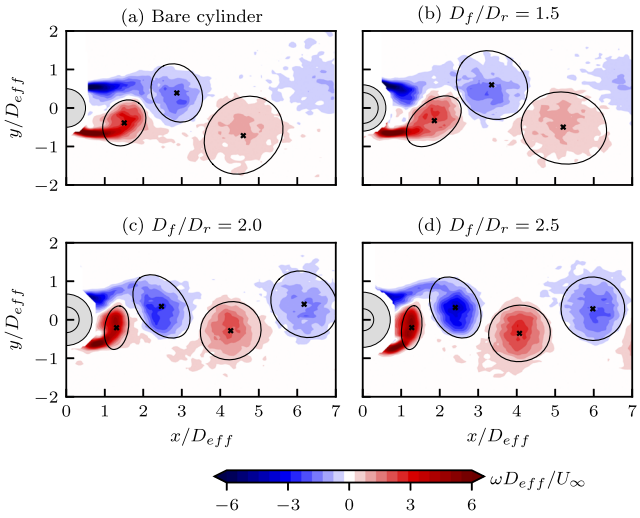


FIG. 10. Comparison of the phase-resolved vorticity field downstream of the cylinders at a phase angle of ϕ = 180° during excitation of acoustic resonance.

are consistent in size and are not distorted by small scale structures. The circulation Γ inside each bounded region S of vorticity $\vec{\omega}$ was calculated as

$$\Gamma = \sum_{i,j} \omega_{ij} \Delta A_{ij}, \tag{13}$$

where ω_{ij} and ΔA_{ij} are the discrete vortices and the corresponding areas within the bounded region, respectively. The regions of vorticity are identified starting one diameter downstream of the cylinder to omit the separating shear layer. In Fig. 10, the identified vortices are shown for the phase ϕ = 180°. Figure 10 also shows that adding fins of different diameter ratios results in vorticity regions with different topologies than the bare cylinder. Increasing diameter ratios (D_f/D_r) results in the formation of vortex cores closer to the cylinder. Previous investigations[12,21] reported a reduction in the vortex formation length downstream of the finned cylinders in the absence of acoustic resonance excitation, as a result of the flow acceleration between the fins and faster shear layer roll-up. Under the influence of the cross-flow oscillation imposed by the acoustic field, the region of the vortex formation is expected to move closer toward the cylinder surface. Moreover, the distribution of vortices in the vortex core becomes more compact downstream of the finned cylinders with higher D_f/D_r as opposed to the elongated structures shown for the bare cylinder in Fig. 10. The compact distribution of the vortices has a significant effect on the induced velocity fluctuations, as will be discussed later.

The evolution of the strength of the vortices based on the circulation is plotted in Fig. 11. This figure includes circulation values calculated from the vortex cores detected at all phases, which provides data for a continuous stream of vortices. Circulation values are normalized using the effective diameter D_{eff} and the free-stream velocity U_∞. The continuous flux of vortices advected from the surface toward the shear layer causes a rapid increase in the circulation during the formation of the vortices until it saturates. After that,

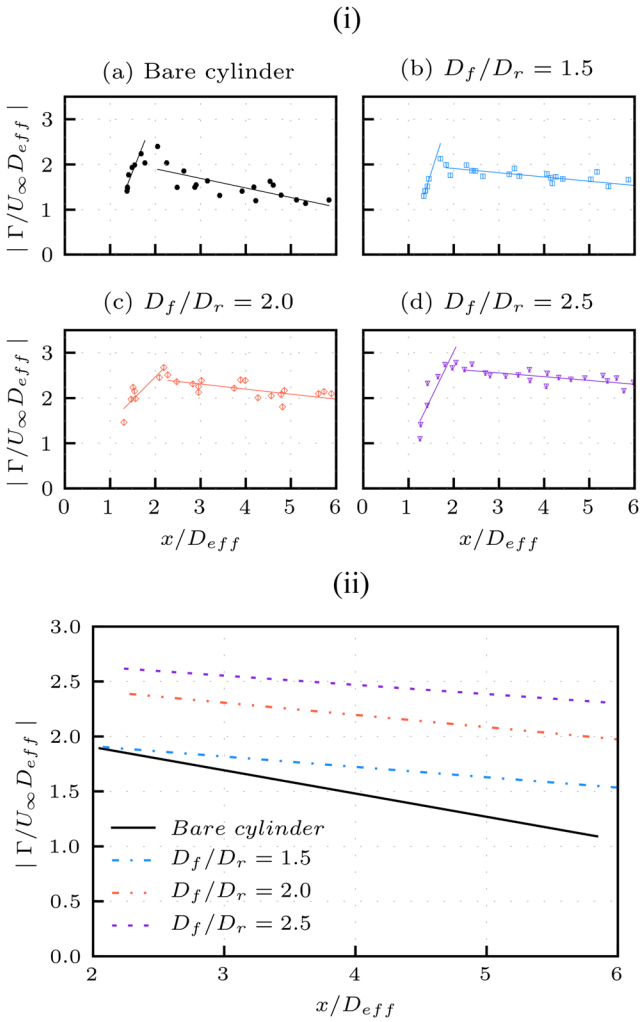


FIG. 11. The effect of the fin-to-root diameter ratio on the vortex strength along the streamwise direction downstream of the cylinders. (i) Development of the vortex strength downstream of each case during acoustic resonance excitation and (ii) comparison of the investigated cases.

the strength of the vortex core drops significantly, indicating that the vortex is being shed from the shear layer, leaving the vortex formation region. After the detachment of the vortex, the strength decreases gradually as the vortex core moves downstream due to the viscous diffusion and vorticity annihilation. The strength of the vortices follows a similar trend in the wake of the finned cylinders. The strength of the vortex cores gradually increases with the increase in the fin diameter ratio. The comparison of the strength of the vortices is shown in Fig. 11(ii) after the detachment of the vortices. The peak magnitude in the formation region for all the finned cylinder cases is higher than that for the bare cylinder, although the free-stream flow velocity is lower. This indicates that the fins have a significant influence on how the vortices are separated and shed, which suggests that the surface geometry of the fins, in addition to the influence

Published under license by AIP Publishing

of the acoustic field, plays a role in the development of the vortex cores. In the absence of the acoustic resonance excitation, the strength of the vortices in the wake of the finned cylinders is also found to be significantly higher than that of the bare cylinder.[12] This finding bolsters the argument that the flow between the fins largely dictates the strength of the vortices in the near wake with an amplification of the effect occurring in the presence of the reciprocating acoustic particle velocity. The strength of the wake vortices for the finned cylinders remains significantly higher over the whole downstream extent. Moreover, the decay rate for circulation downstream of the finned cylinders is lower than that for the bare cylinder. The increased strength of the vortices over the large downstream region is likely to result from the enhanced coherence of the vortex shedding. Moreover, the acoustic particle velocity also exhibits a higher magnitude over the large downstream region, as shown later. The resulting increase in the amplitude of the reciprocating acoustic field would provide feedback to create more organized vortex shedding and, as a result, stronger vortex cores. Because of the characteristics of the trapped acoustic mode, the acoustic particle velocity is higher close to the cylinder surface and is gradually weakened further away from the cylinder. Therefore, the formation of a stronger vortex close to the cylinder is crucial to the effectiveness of the energy transfer mechanism from the flow field to the acoustic field.

It is of interest to look into the trajectories of the shed vortices and their convection velocity (u_c) to understand the comprehensive vortex dynamics in the wake. The trajectories of the vortices located at the positive transverse position from all the phases are plotted in Fig. 12(a). The trajectories are obtained from the coordinates of the vortex centroid, as shown in Fig. 10. The centroid of the vortices exhibits a similar position near the formation region for all the cylinders. After the vortices shed and convected downstream, the trajectories show a distinct variation. The vortices in the wake of the bare cylinder tend to move away from the wake centerline as they travel downstream. The vortices in the wake of the finned cylinder with $D_f/D_r = 1.5$ exhibit a similar trend. In contrast, vortices tend to remain closer to the wake centerline as the diameter ratio of the finned cylinder increases. As will be discussed later, the magnitude of the acoustic particle velocity during resonance remains higher downstream of the finned cylinder with larger diameter ratios compared to that of the bare cylinder. Therefore, the tendency of the vortices to remain close to the wake centerline is likely to result from the entrainment by the acoustic particle velocity, which is largest at the antinode near the wake centerline. The convection velocity of the vortices, which is obtained as the streamwise velocity at the vortex centroid, downstream of the cylinders is shown in Fig. 12(b). Although the excitation of the peak acoustic resonance occurs at different free-stream flow velocities (see Fig. 7), the convection velocity converges to a similar value of $u_c/U_\infty \approx 0.82$ at the downstream end for all the cylinders. The convection velocity is expected to result in a similar magnitude since all the cases become locked-in to the same frequency of the acoustic mode. This is in contrast to the findings of the reduced convection velocity in the wake of the finned cylinders without the acoustic resonance condition.[12] The increase in convection velocity signifies the effect of the feedback imposed by the acoustic field under the resonance excitation. Another interesting observation is the significant increase in the convection velocity near the vortex formation region downstream of the higher diameter ratio finned cylinders. The reason for this can be understood by considering the unsteady Coriolis force, $\rho(\vec{\omega}\times\vec{u}_a)$. The strength of the vortices, as well as the acoustic particle velocity, is found to increase significantly in the vicinity of the higher diameter ratio finned cylinders. As a result, the magnitude of the unsteady Coriolis force is expected to increase. The unsteady Coriolis force is perpendicular to both the acoustic field and the vorticity vector and acts as an unbalanced force in the streamwise direction, which would produce an acceleration in the same direction.[42] Therefore, the significant increase in the convection velocity in the vicinity of the finned cylinder with a higher diameter ratio is attributed to the enhanced fluctuating Coriolis force.

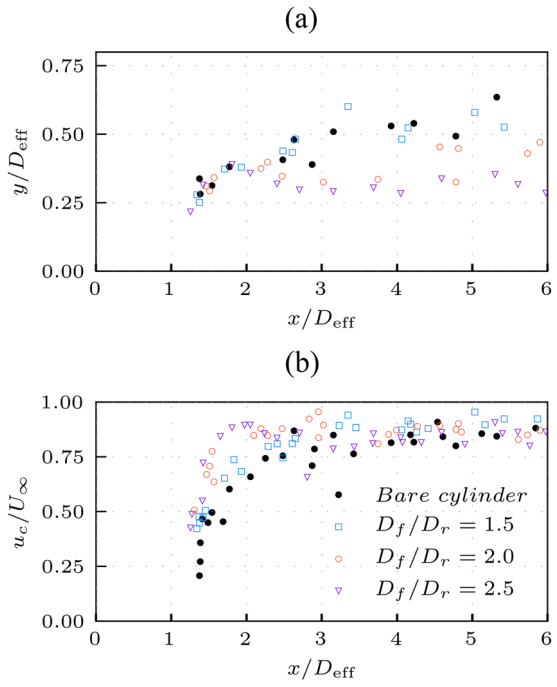


FIG. 12. (a) Streamwise evolution of the trajectories of the vortex centers. (b) Convection velocity in the wake of the cylinders during acoustic resonance excitation.

In Fig. 13, the phase-locked transverse velocity fluctuation v' corresponding to the flow instant with the maximum acoustic particle velocity is shown. The velocity fluctuation is computed by subtracting the time-averaged transverse velocity from the phase-resolved transverse velocity at $\phi = 0°$. For all finned cylinder cases, the first peak of v' is higher than that for the bare cylinder, and the lobe structures of the fluctuating velocity move closer to the cylinder. The next few transverse velocity fluctuations in the wake of the finned cylinder with $D_f/D_r = 1.5$ have a slightly higher magnitude than the bare cylinder. As the diameter ratio D_f/D_r increases, the intensity of the fluctuating velocity field increases, reaching up to 88% of the free-stream velocity in the near wake, indicating the presence of strong resonance excitation downstream of the large D_f/D_r, despite the lower Reynolds numbers. At this point, we can recall that vortices in the wake of the higher diameter ratio finned cylinders show a more compact distribution after it is advected, as shown in Fig. 10. The unsteady velocity field during resonance is

Published under license by AIP Publishing

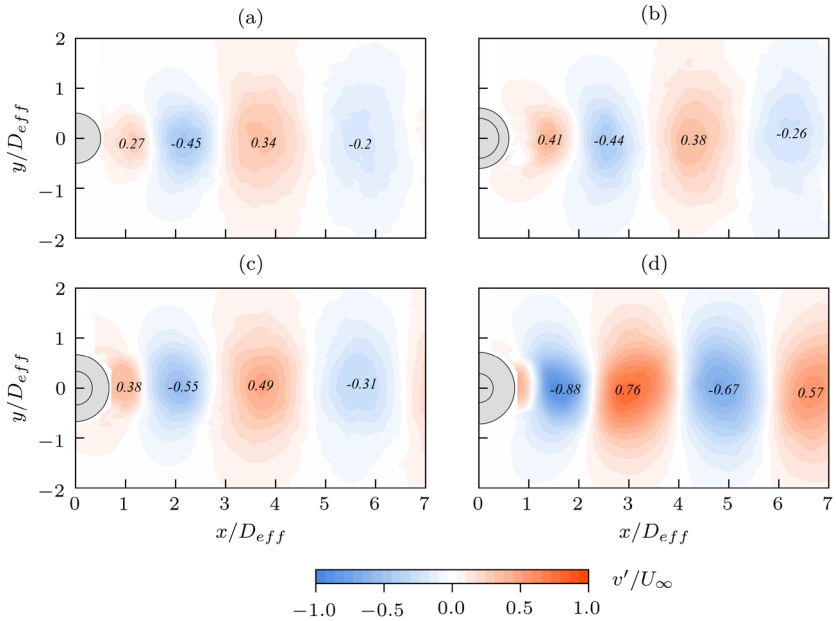


FIG. 13. Effect of the fin-to-root diameter ratio on the normalized transverse velocity fluctuation (v') at phase angle ϕ = 0° of the acoustic resonance pressure cycle. (a) Bare cylinder, (b) D_f/D_r = 1.5, (c) D_f/D_r = 2.0, and (d) D_f/D_r = 2.5.

a combination of the fluctuating velocity field induced by the vorticity and the unsteady potential flow, which describes the reciprocating sound field. Nelson, Halliwell, and Doak[42] used theoretical modeling to describe flow–acoustic interaction and found that the distribution of the vorticity and the radius of the vortex core significantly influence the level of velocity fluctuations. The induced velocity of the vortices is found to increase as the vorticity distribution becomes more tightly packed. Thus, the vortex core radius precedes over the strength that determines the induced velocity fluctuations by the vortices. The increase in unsteady velocity fluctuation with more compact vortices, as found in the present study, tends to agree with this observation. Therefore, a significant increase in the amplitude of the unsteady cross-flow velocity away from the cylinder is attributed to be mainly caused by the velocity induced by vortices. The increased fluctuation in the cross component of the flow velocity can exacerbate the excitation of acoustic resonance by providing more energy to initiate the feedback mechanism.

B. Vortex dynamics along the span of the cylinders

Figure 14 shows the effect of the acoustic resonance excitation on the spanwise structures of the vortices for the cases of a bare cylinder and a finned cylinder with a diameter ratio of D_f/D_r = 2.0. The spanwise structure is compiled from measurements of the vorticity in the x–y planes with a spacing of $0.5D_{\text{eff}}$ in the spanwise direction at the same exact instant of the coupled flow/acoustic cycle. The 3D plot shows the isosurfaces of the normalized vorticity at values between $\omega D/U_\infty$ = −0.75 and 0.75. Without the excitation of acoustic resonance, instabilities result in vortex dislocations between spanwise cells of different frequencies when the primary vortices move out of phase with each other and the wake pattern is dominated by the streamwise vortex pairs spaced by a distance of about one cylinder diameter.[29] Therefore, measurements were carried out to cover a distance of three-cylinder diameters in the spanwise direction during the excitation of acoustic resonance. The 3D isosurfaces in Fig. 14 show notably straight, consistent vortex cores along the spanwise direction for both cases. The features of the vorticity field discussed in Figs. 8–10 also reflected the uniformity of the vortex core along the span. This can be further seen from the contours shown at different spanwise locations in Fig. 14. For each case, only slight differences can be observed between the vorticity field. Similar observations of vortex synchronization have been indicated for other configurations. For example, Yokoyama, Kitamiya, and Iida[31] showed that imposing acoustic resonance on a cascade of flat plates leads to synchronized vortex shedding and a shorter vortex formation length. It is evident from Fig. 14 that self-excited acoustic resonance can have a similar effect on the structures of the wake downstream of cylinders. It can also be seen that the structures are more organized and consistent in the case of the finned cylinder, which is associated with a stronger resonance excitation and the effect of the flow between the fins. The synchronization of vortex shedding over the spanwise direction at a high Reynolds number is a fundamental change to the wake flow and an important consequence of the strong acoustic resonance. The increased correlation of the vortex cores along the cylinder's span during the resonance excitation suggests the existence of wake flow, which is dominantly two-dimensional. Several studies[13,15] in the literature have utilized the two-dimensional numerical simulation to study the effect of the acoustic resonance excitation in the wake of the bare cylinder, which seems reasonable as evident from the present results. Moreover, the current results emphasize the fact that it is possible to use the assumption of the two-dimensional flow field in numerical simulations, which can be coupled with a two-dimensional acoustic field to study the acoustic resonance excitation in complex flow geometries with reasonable accuracy.

Published under license by AIP Publishing

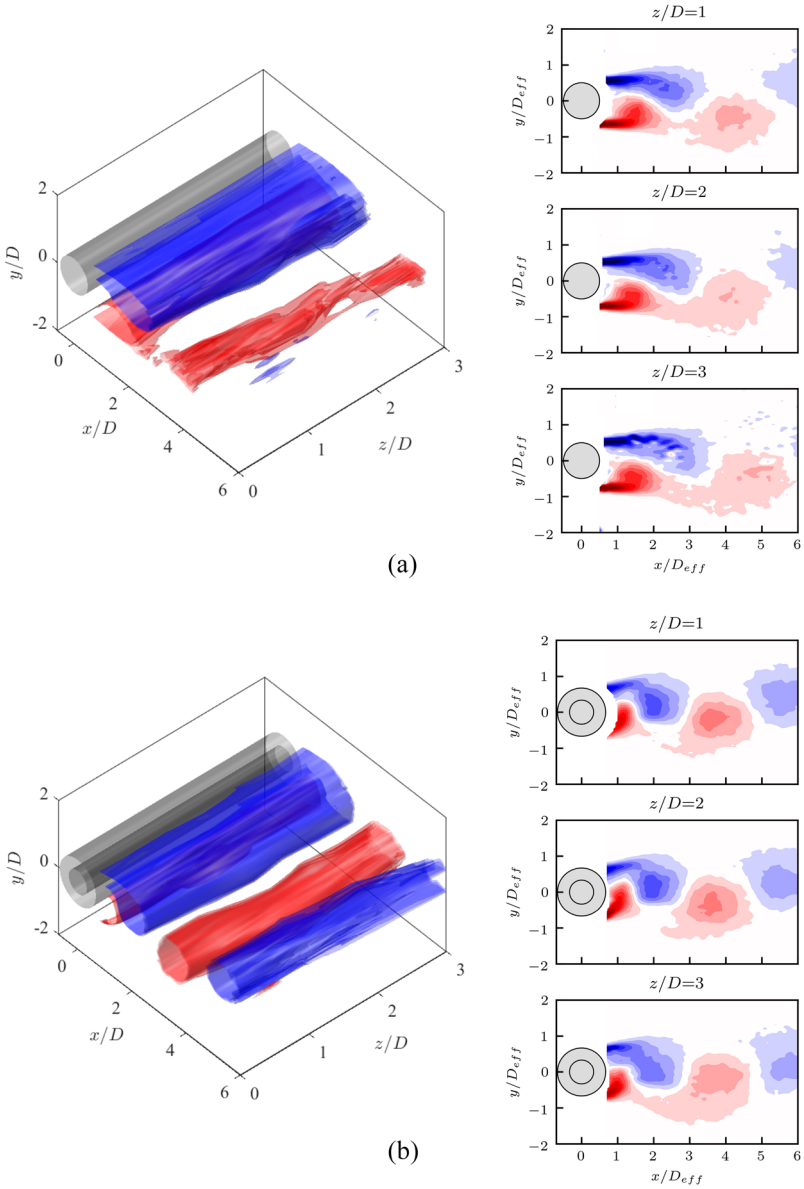


FIG. 14. Iso-surface of the vorticity along the span of the cylinder at phase angle ϕ = 90° of the acoustic resonance cycle in the wake of (a) a single bare cylinder and (b) a finned cylinder with D_f/D_r = 2.0.

V. AEROACOUSTIC ENERGY TRANSFER

In this section, the aeroacoustic energy transfer in the wake of the cylinders due to the feedback mechanism between the flow field and the resonant sound field is discussed. Figure 15 shows the components used to calculate the acoustic energy production Π using the algorithm shown in Fig. 3 for the bare cylinder and the finned cylinder with D_f/D_r = 2.0, corresponding to the phase, $\phi = 0^\circ$, of the acoustic pressure cycle. The acoustic particle velocity field $u_a(x, y)$, the vorticity $\omega(x, y)$, and the velocity $\vec{U}(x, y)$ of the flow field are used to calculate the acoustic energy production using Eq. (7). At this phase, the acoustic particle velocity field $u_a(x, y)$ is at its maximum amplitude, traveling toward the positive transverse direction. The magnitude of the acoustic particle velocity is higher close to the cylinder surface for both cases, as evident from Figs. 15(a) and 15(b). Therefore, the strong aeroacoustic coupling is expected to occur in this region. The acoustic particle velocity also exhibits a higher value away from the surface of the finned cylinder compared to the bare cylinder. The vorticity field corresponding to the same phase is shown in Figs. 15(c) and 15(d) for the bare cylinder and the finned cylinder, respectively. The instantaneous acoustic power at this phase is calculated using the expression in Eq. (7), and the distribution is shown in Figs. 15(e) and 15(f). Acoustic power denotes the rate at which the flow does work on the acoustic field. Therefore, the positive value shows the region where the acoustic energy is generated, and the negative value denotes the region

Published under license by AIP Publishing

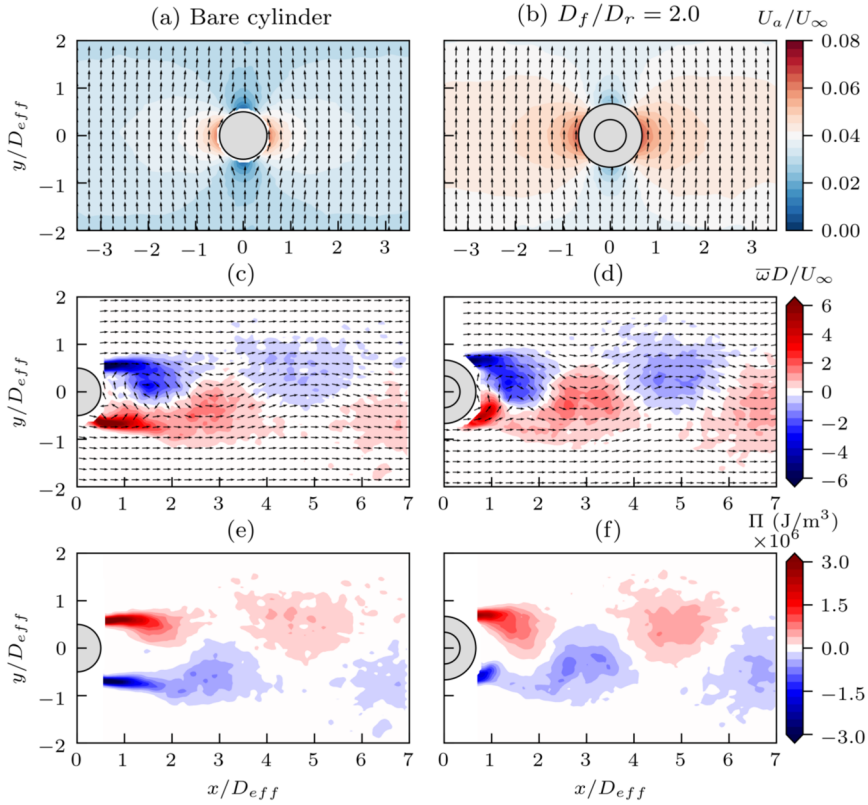


FIG. 15. Instantaneous acoustic power in the wake of the bare cylinder and finned cylinder with D_f/D_r = 2.0 at phase ϕ = 0°. [(a) and (b)] Acoustic particle velocity, [(c) and (d)] instantaneous vorticity, and [(e) and (f)] instantaneous acoustic power.

where the acoustic energy is absorbed by the unsteady flow. As evident from Figs. 15(e) and 15(f), vortex cores circulating clock-wise interact with the acoustic field to generate sound energy, whereas the vortex cores circulating counter-clockwise cause sound absorption. Moreover, due to lock-in, the two fields are at the same phase in the opposite side of the cycle, when the acoustic particle velocity and the flow field are mirrored, leading to a continuous cycle of the acoustic energy production. Acoustic sources and sinks with higher intensity are located near the shear layer region, and the intensity decreases as the vortices travel downstream. The vortices do not generate or absorb acoustic energy at the instants of the acoustic pressure cycle corresponding to the phases, $\phi = 90°$ and 270°, as the acoustic particle velocity magnitude is zero.

It is instructive to compare the net aeroacoustic energy transfer over one acoustic pressure cycle among the cylinders. The net energy over the acoustic pressure cycle can be obtained by integrating the instantaneous acoustic power distribution of the eight phases. Figures 16(a), 16(c), 16(e), and 16(g) show the distribution of the aeroacoustic sources and sinks derived from the net aeroacoustic energy in the wake of the cylinders. A strong acoustic source is located in the vicinity of the bare cylinder and extends over the vortex formation region, as evident from Fig. 16(a). Acoustic sources and sinks are then arranged in an alternating pattern similar to the numerical observations of Mohany and Ziada[13] in the case of a single bare cylinder. The net distribution of the acoustic sources and sinks in the wake of the finned cylinders in Figs. 16(c), 16(e), and 16(g) exhibits distinct characteristics. For the finned cylinder cases, the source and sink distributions move closer toward the cylinder location as the diameter ratio increases, which is consistent with the shorter vortex formation region. Therefore, cylinders with a higher diameter ratio (D_f/D_r) induce a higher number of sources and sinks within the same distance into the wake. Moreover, the acoustic energy production within the sources and sinks increases significantly as the diameter ratio increases, implying stronger flow-acoustic coupling. The increase in the aeroacoustic energy generation is consistent with the increase in the acoustic resonance level found in the case of the finned cylinders.

To quantify the net acoustic energy transfer from the flow field to the acoustic field, the accumulated energy production at each downstream location is integrated vertically within ±2 D_{eff}. The distribution of the integrated acoustic energy downstream of the cylinders along the streamwise direction is shown in Figs. 16(b), 16(d), 16(f), and 16(h). In the case of the bare cylinder, the net acoustic energy transfer is positive near the cylinder due to the location of a strong acoustic source. The net energy transfer shows alternating positive and negative values due to the location of the sources and sinks in the wake. Compared to the case of the bare cylinder, the acoustic energy production is only slightly enhanced when a finned cylinder with D_f/D_r = 1.5 is used. Increasing the diameter ratio to D_f/D_r = 2.0 causes a significant increase in the peaks and troughs of the acoustic energy production, which corresponds to the stronger distribution of acoustic sources and sinks. This higher

Published under license by AIP Publishing

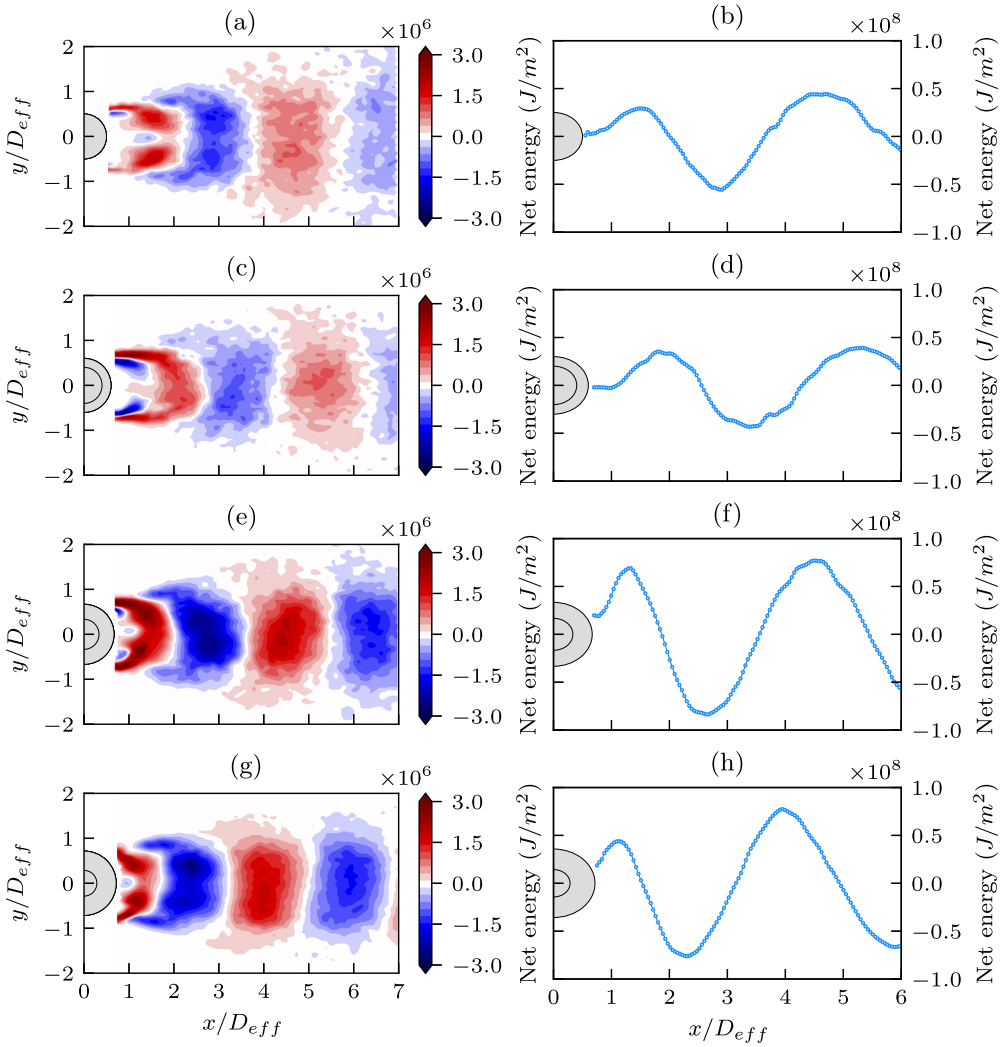


FIG. 16. Comparison of the aeroacoustic energy transfer in the wake of the cylinders. [(a) and (b)] Bare cylinder, [(c) and (d)] D_f/D_r = 1.5, [(e) and (f)] D_f/D_r = 2.0, and [(g) and (h)] D_f/D_r = 2.5.

energy exchange between the flow and the acoustic fields in the wake of the finned cylinder with D_f/D_r = 2.0 explains the stronger resonance excitation observed for cylinders with a higher diameter ratio. This increase is a result of the combined effects of fins on the flow development and the acoustic fields when the diameter ratio of the fins is increased. First, even though acoustic resonance excitation occurs at lower flow velocities, the higher diameter ratio is associated with the shedding of stronger, more organized vortex cores, and thus, the energy production is enhanced. Second, the presence of fins was found to enhance the amplitude of the acoustic particle velocity as seen in Figs. 15(a) and 15(b) so that the acoustic field can produce more energy at locations further downstream. The combined effect of those two factors resulted in a significant increase in the production rate of acoustic power (Π), although the incoming flow velocity was lower at the peak of the acoustic resonance excitation.

These observations point to a very crucial role played by the changes introduced to the wake flow, the acoustic field, and the three-dimensionality of the shed vortices. The current understanding of the self-excitation mechanisms of acoustic resonance is based on observations collected from bare cylinder cases. Finned cylinders, which are common in engineering applications, were found to produce a stronger acoustic resonance at lower flow velocities, which asserts the importance of taking the effect of the fin parameters and the changes introduced to the excitation mechanism of acoustic resonance into account.

VI. CONCLUSION

In this work, a hybrid experimental–numerical method was used to investigate the excitation of acoustic resonance in the wake

Published under license by AIP Publishing

of finned cylinders in cross-flow. Finned cylinders with the same effective diameter, fin pitch, and thickness, but with different fin-to-root diameter ratios were rigidly fixed in cross-flow at the location of the acoustic pressure node (i.e., acoustic particle velocity anti-node of the first acoustic cross-mode). In all cases, acoustic resonance was self-excited at a flow velocity that corresponds to the coincidence of the vortex shedding frequency and the acoustic cross-mode of the duct. Despite having the same effective diameter, the excitation of acoustic resonance yields distinct characteristics for the finned cylinders. The presence of fins causes significant changes in the wake vortex shedding characteristics compared to the case of a bare cylinder, affecting the acoustic resonance excitation. In particular, the flow entrainment between the fins increases the strength of the periodic vortex shedding in the wake of finned cylinders, an effect that becomes more pronounced with increasing diameter ratios. As a result, finned cylinders are able to excite acoustic resonance at flow velocities lower than those for the case of bare cylinders. On the other hand, finned cylinders undergo a narrower lock-in region and a higher normalized acoustic pressure during resonance excitation compared to the case of the bare cylinder. Therefore, observations of the characteristics of acoustic resonance excitation studied using bare cylinders with the same effective diameter as the finned cylinders could be misleading. Furthermore, the distribution of acoustic sources and sinks in the wake is obtained using phase-locked experimental data of the flow field in addition to the resonant acoustic field from numerical simulations, indicating that aeroacoustic coupling in the wake of the finned cylinders is stronger than that for the bare cylinder. The observed change in the aeroacoustic energy transfer is consistent with the intrinsic flow dynamics that arise as a result of the addition of fins. Finally, flow measurements were carried out at different locations along the span of bare and finned cylinders during resonance. The results show that the vortices exhibit a uniform distribution in the spanwise direction in the presence of self-excited acoustic resonance, which indicates that using a two-dimensional model to study the mechanism of acoustic resonance excitation can allow significant progress toward effective methods to control its hazardous consequences.

ACKNOWLEDGMENTS

The authors would like to acknowledge the financial support provided by the Natural Sciences and Engineering Research Council of Canada (NSERC).

DATA AVAILABILITY

The data that support the findings of this study are available from the corresponding author upon reasonable request.

REFERENCES

[1]R. D. Blevins and M. M. Bressler, "Experiments on acoustic resonance in heat exchanger tube bundles," J. Sound Vib. **164**, 503–533 (1993).
[2]A. Oengören and S. Ziada, "An in-depth study of vortex shedding, acoustic resonance and turbulent forces in normal triangle tube arrays," J. Fluids Struct. **12**, 717–758 (1998).
[3]S. Ziada, A. Oengören, and A. Vogel, "Acoustic resonance in the inlet scroll of a turbo-compressor," J. Fluids Struct. **16**, 361–373 (2002).
[4]R. Parker and D. C. Pryce, "Wake excited resonances in an annular cascade: An experimental investigation," J. Sound Vib. **37**, 247–261 (1974).
[5]H. M. Al-Muslim, N. I. Al-Nasri, and M. Y. Al-Hashem, "The danger of piping failure due to acoustic-induced fatigue in infrequent operations: Two case studies," J. Pressure Vessel Technol. **135**, 064501 (2013).
[6]T. Lato and A. Mohany, "Passive damping of pressure pulsations in pipelines using Herschel-Quincke tubes," J. Sound Vib. **448**, 160–177 (2019).
[7]P. Wang and Y. Liu, "Intensified flow dynamics by second-order acoustic standing-wave mode: Vortex-excited acoustic resonances in channel branches," Phys. Fluids **31**, 035105 (2019).
[8]P. Wang, Y. Deng, and Y. Liu, "Vortex dynamics during acoustic-mode transition in channel branches," Phys. Fluids **31**, 085109 (2019).
[9]P. Wang, Y. Deng, and Y. Liu, "Vortex-excited acoustic resonance in channel with coaxial side-branches: Vortex dynamics and aeroacoustic energy transfer," Phys. Fluids **30**, 125104 (2018).
[10]S. Ziada, "Flow-excited acoustic resonance in industry," J. Pressure Vessel Technol. **132**, 015001 (2010).
[11]NRC, Additional Flow-Induced Vibration Failures after a Recent Power uprate, NRC Information Notice 2002-26, Supplement 2 (US Nuclear Regulatory Commission, Washington, DC, USA, 2004).
[12]M. R. Islam and A. Mohany, "Vortex shedding characteristics in the wake of circular finned cylinders," Phys. Fluids **32**, 045113 (2020).
[13]A. Mohany and S. Ziada, "Numerical simulation of the flow-sound interaction mechanisms of a single and two-tandem cylinders in cross-flow," J. Pressure Vessel Technol. **131**, 031306 (2009).
[14]A. Mohany and S. Ziada, "Effect of acoustic resonance on the dynamic lift forces acting on two tandem cylinders in cross-flow," J. Fluids Struct. **25**, 461–478 (2009).
[15]Z. Hong, X. Wang, X. Jing, and X. Sun, "Frequency lock-in mechanism in flow-induced acoustic resonance of a cylinder in a flow duct," J. Fluid Mech. **884**, A42 (2020).
[16]N. Arafa and A. Mohany, "Flow-excited acoustic resonance of isolated cylinders in cross-flow," J. Pressure Vessel Technol. **138**, 011302 (2016).
[17]M. Shaaban and A. Mohany, "Characteristics of acoustic resonance excitation by flow around inline cylinders," J. Pressure Vessel Technol. **141**, 051301 (2019).
[18]M. Shaaban and A. Mohany, "Phase-resolved PIV. Measurements of flow over three unevenly spaced cylinders and its coupling with acoustic resonance," Exp. Fluids **60**, 71 (2019).
[19]M. Shaaban and A. Mohany, "Experimental study of the self-excited resonance effect on the dynamic lift and flow structure around inline cylinders," J. Fluids Struct. **96**, 103015 (2020).
[20]J. McClure and S. Yarusevych, "Vortex shedding and structural loading characteristics of finned cylinders," J. Fluids Struct. **65**, 138–154 (2016).
[21]N. Arafa and A. Mohany, "Wake structures and acoustic resonance excitation of a single finned cylinder in cross-flow," J. Fluids Struct. **86**, 70–93 (2019).
[22]M. Eid and S. Ziada, "Vortex shedding and acoustic resonance of single and tandem finned cylinders," J. Fluids Struct. **27**, 1035–1048 (2011).
[23]N. Arafa and A. Mohany, "Aeroacoustic response of a single cylinder with straight circular fins in cross-flow," J. Pressure Vessel Technol. **137**, 051301 (2015).
[24]M. S. Howe, "Contributions to the theory of aerodynamic sound, with application to excess jet noise and the theory of the flute," J. Fluid Mech. **71**, 625–673 (1975).
[25]M. S. Howe, "The dissipation of sound at an edge," J. Sound Vib. **70**, 407–411 (1980).
[26]S. Finnegan, C. Meskell, and S. Ziada, "Experimental investigation of the acoustic power around two tandem cylinders," J. Pressure Vessel Technol. **132**, 041306 (2010).
[27]A. Mohany, D. Arthurs, M. Bolduc, M. Hassan, and S. Ziada, "Numerical and experimental investigation of flow-acoustic resonance of side-by-side cylinders in a duct," J. Fluids Struct. **48**, 316–331 (2014).

Published under license by AIP Publishing

[28]C. H. K. Williamson, "The existence of two stages in the transition to three-dimensionality of a cylinder wake," Phys. Fluids **31**, 3165–3168 (1988).
[29]M. Zhao, J. Thapa, L. Cheng, and T. Zhou, "Three-dimensional transition of vortex shedding flow around a circular cylinder at right and oblique attacks," Phys. Fluids **25**, 014105 (2013).
[30]M. Hayakawa and F. Hussain, "Three-dimensionality of organized structures in a plane turbulent wake," J. Fluid Mech. **206**, 375–404 (1989).
[31]H. Yokoyama, K. Kitamiya, and A. Iida, "Flows around a cascade of flat plates with acoustic resonance," Phys. Fluids **25**, 106104 (2013).
[32]L.-H. Feng, G.-P. Cui, and L.-Y. Liu, "Two-dimensionalization of a three-dimensional bluff body wake," Phys. Fluids **31**, 017104 (2019).
[33]C. Norberg, "Pressure distributions around a circular cylinder in cross-flow," in *Proceedings of the Symposium on Bluff Body Wakes and Vortex-Induced Vibrations* (Monash University, Melbourne, Australia, 2002), pp. 1–4, available at https://lup.lub.lu.se/search/publication/594296.
[34]W. A. Mair and P. D. F. Jones, "Vortex shedding from finned tubes," J. Sound Vib. **39**, 293–296 (1975).
[35]N. Arafa, A. Tariq, A. Mohany, and M. Hassan, "Effect of cylinder location inside a rectangular duct on the excitation mechanism of acoustic resonance," Can. Acoustics **42**, 33–40 (2014) available at https://jcaa.caa-aca.ca/index.php/jcaa/article/view/2609.
[36]A. Mohany and S. Ziada, "Flow-excited acoustic resonance of two tandem cylinders in cross-flow," J. Fluids Struct. **21**, 103–119 (2005).
[37]W. K. Blake, *Mechanics of Flow-Induced Sound and Vibration*, General Concepts and Elementary Sources Vol. 1 (Academic Press, 2017).
[38]M. S. Howe, "Sound generated by fluid-structure interactions," Comput. Struct. **65**, 433–446 (1997).
[39]M. Raffel, C. E. Willert, F. Scarano, C. J. Kähler, S. T. Wereley, and J. Kompenhans, *Particle Image Velocimetry: A Practical Guide* (Springer, 2018).
[40]J. C. Hunt, A. A. Wray, and P. Moin, "Eddies, streams, and convergence zones in turbulent flows," in *Proceedings of the 1988 Summer Program* (Center for Turbulence Research, Standford University, 1988).
[41]E. Marble, C. Morton, and S. Yarusevych, "Vortex dynamics in the wake of a pivoted cylinder undergoing vortex-induced vibrations with elliptic trajectories," Exp. Fluids **59**, 78 (2018).
[42]P. A. Nelson, N. A. Halliwell, and P. E. Doak, "Fluid dynamics of a flow excited resonance, part II: Flow acoustic interaction," J. Sound Vib. **91**, 375–402 (1983).

Published under license by AIP Publishing